Inorganic Chemistry
Article

Inorg. Chem. **2010**, *49*, 5453–5459 **5453**
DOI: 10.1021/ic902553f

Interfacial Confined Formation of Mesoporous Spherical TiO_2 Nanostructures with Improved Photoelectric Conversion Efficiency

Wei Shao,[†] Feng Gu,[*,†,‡] Chunzhong Li,[*,†] and Mengkai Lu[‡,§]

[†]*Key Laboratory for Ultrafine Materials of Ministry of Education, School of Materials Science and Engineering, East China University of Science and Technology, Shanghai 200237, China,* [‡]*Department of Physics and Center for NanoScience (CeNS), Ludwig-Maximilians University (LMU), Munich 80799, Germany, and* [§]*State Key Laboratory of Crystal Materials, Shandong University, Jinan 250100, China*

Received December 22, 2009

Uniform mesoporous TiO_2 nanospheres were successfully developed via an interfacial confined formation process for application in dye-sensitized solar cells. The mesoporous spherical structures greatly promote the dye-loading capacity, electron transfer, and light scattering, resulting in remarkable enhancement of the cell performance. The designed interfacial platform caused a reaction-limited aggregation of the TiO_2 nanocrystals, resulting in the formation of mesoporous spherical nanostructures with sphere diameter of 216 nm and pore size of 8 nm. The oriented attachment of adjacent TiO_2 nanocrystals facilitated the electron transfer process when the mesoporous TiO_2 nanospheres were used as electrode films. The dye coverage was enhanced remarkably in the mesoporous spherical TiO_2 samples. Owing to the enhanced light-harvesting efficiency, solar conversion efficiency was enhanced about 30% for the dye-sensitized solar cell (DSSC) based on mesoporous spherical TiO_2 in comparison with that made by commercial TiO_2 nanoparticles.

Introduction

Currently, exploration of environmentally clean alternate energy resources has become one of the most important topics in the fields of science and technology to meet the demand of clean energy.[1−3] Since the breakthrough work by Grätzel in 1991, dye-sensitized solar cell (DSSC) has opened a challenging new field as a potential low-cost alternative to conventional solar cells owing to the remarkably high power-conversion efficiency combined with low-tech fabrication processes.[4−6] As technology progressed, the conversion efficiency of such cells was steadily increased, and now up to 11% conversion efficiency has been achieved.[7,8] With respect to the DSSC, one of the main factors that hampered its widespread practical use is the low surface area of the thin-film electrodes. Photoelectrode materials, such as mesoporous titania, with high surface area are necessary to effectively adsorb the dye and achieve a high photocurrent.[4,9−18] So far, there have been only a few reports on processing strategies designed to provide markedly enhanced surface activities and photocurrent efficiency for thin-film photoelectrodes. Zukalova et al. prepared ordered mesoporous TiO_2 nanocrystalline films via layer-by-layer deposition with Pluronic P123 as template and found that the mesoporous TiO_2 films showed

*To whom correspondence should be addressed. E-mail: gufeng@ecust.edu.cn (F.G.); czli@ecust.edu.cn (C.L.).

(1) Dresselhaus, M. S.; Thomas, I. L. *Nature* **2001**, *414*, 332–337.
(2) Kongkanand, A.; Vinodgopal, K.; Kuwabata, S.; Kamat, P. V. *J. Phys. Chem. B* **2006**, *110*, 16185–16188.
(3) Kamat, P. V. *J. Phys. Chem. C* **2007**, *111*, 2834–2860.
(4) Oregan, B.; Grätzel, M. *Nature* **1991**, *353*, 737–740.
(5) Durr, M.; Schmid, A.; Obermaier, M.; Rosselli, S.; Yasuda, A.; Nelles, G. *Nat. Mater.* **2005**, *4*, 607–611.
(6) Grätzel, M. *Nature* **2001**, *414*, 338–344.
(7) Grätzel, M. *J. Photochem. Photobiol., A* **2004**, *164*, 3–14.
(8) Grätzel, M. *Chem. Lett.* **2005**, *34*, 8–13.
(9) Fan, S. Q.; Cao, R. J.; Xi, Y. X.; Gao, M.; Wang, M. D.; Wang, G.; Kim, C. W.; Kim, J. J.; Baik, C. *Optoelectron. Adv. Mater.* **2009**, *3*, 101–105.
(10) Yang, L.; Lin, Y.; Jia, J. G.; Xiao, X. R.; Li, X. P.; Zhou, X. W. *J. Power Sources* **2008**, *182*, 370–376.
(11) Lancelle-Beltran, E.; Prene, P.; Boscher, C.; Belleville, P.; Buvat, P.; Lambert, S.; Guillet, F.; Boissiere, C.; Grosso, D.; Sanchez, C. *Chem. Mater.* **2006**, *18*, 6152–6156.
(12) Hu, L. H.; Dai, S. Y.; Weng, J.; Xiao, S. F.; Sui, Y. F.; Huang, Y.; Chen, S. H.; Kong, F. T.; Pan, X.; Liang, L. Y.; Wang, K. J. *J. Phys. Chem. B* **2007**, *111*, 358–362.
(13) Zukalova, M.; Zukal, A.; Kavan, L.; Nazeeruddin, M. K.; Liska, P.; Grätzel, M. *Nano Lett.* **2005**, *5*, 1789–1792.
(14) Kim, Y. J.; Lee, Y. H.; Lee, M. H.; Kim, H. J.; Pan, J. H.; Lim, G. I.; Choi, Y. S.; Kim, K.; Park, N. G.; Lee, C.; Lee, W. I. *Langmuir* **2008**, *24*, 13225–13230.
(15) Prochazka, J.; Kavan, L.; Zukalova, M.; Frank, O.; Kalbac, M.; Zukal, A.; Klementova, M.; Carbone, D.; Grätzel, M. *Chem. Mater.* **2009**, *21*, 1457–1464.
(16) Kang, S. H.; Choi, S. H.; Kang, M. S.; Kim, J. Y.; Kim, H. S.; Hyeon, T.; Sung, Y. E. *Adv. Mater.* **2008**, *20*, 54–58.
(17) Han, X. G.; He, H. Z.; Kuang, Q.; Zhou, X.; Zhang, X. H.; Xu, T.; Xie, Z. X.; Zheng, L. S. *J. Phys. Chem. C* **2009**, *113*, 584–589.
(18) Alexaki, N.; Stergiopoulos, T.; Kontos, A. G.; Tsoukleris, D. S.; Katsoulidis, A. P.; Pomonis, P. J.; LeClere, D. J.; Skeldon, P.; Thompson, G. E.; Falaras, P. *Microporous Mesoporous Mater.* **2009**, *124*, 52–58.

Published on Web 05/27/2010

enhanced solar conversion efficiency by about 50% compared to traditional films of the same thickness made from randomly oriented anatase nanocrystals.[13] This improvement resulted from a remarkable enhancement of the short circuit photocurrent, because of the huge surface area accessible to both the dye and the electrolyte.[13] These materials have received significant research attention with alkylphosphate surfactants, octadecylamine, and triblock copolymer as structure-directing agents. Such approaches, though successful in the formation of mesoporous TiO_2 films, were both complex and difficult to control. Lately, Kim et al. prepared hierarchical pore generation with nanoporous TiO_2 spheres structures by a two-step process of hydrolysis and hydrothermal reaction. The increment in dye absorption was simply proportional to the surface area of the TiO_2, and it was deduced that the enhanced solar conversion efficiency of the DSSC was closely related with the larger amounts of anchored dye molecules.[19] The two-step experiment is still complex and energy-consuming. Therefore, it is desirable to explore facile routes for the synthesis of mesoporous TiO_2 with promising novel properties, especially, such methods that may be easily controllable, consistently repeatable, mild, and feasible.

In this paper, we demonstrate a one-pot solution method, free of organic structure-directing agents or pretreated substrates for large-scale synthesis of uniform mesoporous spherical TiO_2 nanostructures. Since the size is comparable to the wavelengths of the visible and UV lights, the diffractions on the spheres and the reflections due to the mesostructure would improve the functional properties of TiO_2.[20] The special spherical morphology processes light-scattering characteristics, which can confine the incident light within an electrode and thereby enhances the photocurrent density.[21−24] Except for their role in the actual light scattering, these mesoporous spheres offer additional effect, for instance, electron generation, because dye adsorption is expected to be much more for these particles than for nanocrystalline TiO_2 owing to their much larger surface area.[25] Therefore, the mesoporous spheres we developed offer both light-scattering and electricity-generation properties.

Experimental Section

Synthesis of Mesoporous Spherical TiO_2. In a typical experiment, the stock aqueous solution was first prepared by adding 3.4 mL tetra-*n*-butyl titanate (TBT) to 25.5 mL of *n*-butanol (Aldrich) under rapid stirring for 20 min to obtain transparent stock solution. Then it was dropwise introduced to 100 mL of boric acid aqueous solution (0−1.70M). TBT hydrolyzed at the interface region between *n*-butanol and aqueous solution. After aging at room temperature for 72 h, the precipitate was centrifugally washed with absolute ethanol and distilled water several times to remove possible residual impurities. After being dried in an oven at 60 °C overnight, the sample was calcined at 450 °C (heating rate: 1 °C/min) and kept at this temperature for 3 h.

Preparation of DSSCs. In the fabrication of DSSCs, the normal TiO_2 (commercially Degussa P25) paste was first prepared. A 2.4 g portion of TiO_2 nanopowders was dispersed in acetylacetone ethanol aqueous solution (10 vol %) and ground for 30 min. A 3.2 mL portion of distilled water and 0.04 mL of Triton X-100 (Aldrich) were introduced into the above mixture. After 0.5 h of grinding, the resultant sol was printed onto F-doped SnO_2 conducting glass (Nippon Sheet Glass, SnO_2: F, 15ohm/sq) with an active area of 0.25 cm^2 using the screen printing technique, which was then heated at 450 °C for 30 min. For the bilayer structure, the mesoporous TiO_2 particle layer was deposited by a spin-coating method on annealed P25 TiO_2 films and heated over the same heating profile as previously. The resulting TiO_2 films were immersed in anhydrous ethanol containing 0.5 mM of Ru-dye $(Bu_4N)_2[Ru(Hdcbpy)_2\text{-}(NCS)_2]$ (N719 dye, Solaronix), and kept for 24 h at room temperature. The dye-treated TiO_2 electrodes were rinsed with ethanol and dried under nitrogen flow. Pt counter electrodes were prepared on the FTO glasses using 0.7 mM H_2PtCl_6 solution, followed by heating at 380 °C for 20 min in air. The redox electrolyte used was 0.1 M LiI, 0.05 M I_2, 0.6 M 1, 2-dimethyl-3-propylimidazolium iodide, and 0.5 M 4-*tert*-butylpyridine in dried acetonitrile. The two electrodes were sealed together with a hot-melt polymer film (60 μm thick, Surlyn, DuPont).

Characterization. The X-ray diffraction (XRD) patterns of the samples were measured by using a Japan Rigaku D/max 2550 VB/PC diffractometer with Cu−Kα radiation (λ = 0.15418 nm). A transmission electron microscope (JEM-100CXII) and a high-resolution transmission electron microscope (JEM-2100) were also used to characterize the products. Scanning electron micrograph (SEM) images were taken with a FEI SIRION-200 scanning electron microscope. X-ray photoelectron spectroscopy (XPS) spectra were recorded by a PHI 5000C ESCA spectrometer using Mg Kα radiation ($h\nu$ = 1253.6 eV). The pressure of the analyzer chamber was maintained at 5×10^{-8} Pa. The shift of the binding energy due to relative surface charging was corrected using the C 1s level at 284.6 eV as an internal standard. Nitrogen adsorption−desorption isotherms were measured on an AUTOSORB-1 analyzer (Quantachrome Instruments). Before the measurements, the samples were outgassed at 300 °C for 5 h in vacuum. The pore-size distributions (PSD) were derived from the adsorption and desorption branches of the isotherms using the Barrett−Joyner−Halanda (BJH) method, respectively. The total pore volumes were estimated from the amount adsorbed at the relative pressure of p/p_0 = 0.99 signal point.

The dye was desorbed from the TiO_2 electrodes with a 0.25 cm^2 area and the same thickness of 15 μm by treatment with equal volume of 0.1 M aqueous NaOH solution. The absorbance of the resulting solution was quantified with a Scan UV−vis−NIR spectrophotometer (Varian, Cary 500). A Keithley 2400 source meter and a 500 W xenon lamp (Shanghai Danguang) were used to measure the current−voltage characteristics. The light intensity was adjusted using an irradiatometer (FZ-A, Photoelectric Instrument Factory of Beijing Normal University) to 100 $mW \cdot cm^{-2}$ (the equivalent of one sun at AM1.5G) at the surface of a testing cell. The cell was covered with a piece of heat-protecting glass and a band-pass filter (400−800 nm) to remove ultraviolet and infrared radiation. The current−voltage characteristics of the cell under these conditions were obtained by applying an external potential bias to the cell and measuring the generated photocurrent with the Keithley model 2400 digital source meter (Keithley Instruments, Inc. U.S.A.), generating voltage pulses (typically ±50 mV of 1 s duration) and measuring electrical current through the electrodes. This process was fully automated using Wavemetrics software

(19) Kim, Y. J.; Lee, M. H.; Kim, H. J.; Lim, G.; Choi, Y. S.; Park, N.; Kim, K.; Lee, W. I. *Adv. Mater.* **2009**, *21*, 3668–3673.
(20) Li, H. X.; Bian, Z. F.; Zhu, J.; Zhang, D. Q.; Li, G. S.; Huo, Y. N.; Li, H.; Lu, Y. F. *J. Am. Chem. Soc.* **2007**, *129*, 8406–8407.
(21) Koo, H. J.; Kim, Y. J.; Lee, Y. H.; Lee, W. I.; Kim, K.; Park, N. G. *Adv. Mater.* **2008**, *2*, 195–199.
(22) Wang, Z. S.; Kawauchi, H.; Kashima, T.; Arakawa, H. *Coord. Chem. Rev.* **2004**, *248*, 1381–1389.
(23) Ito, S.; Zakeeruddin, S. M.; Humphry-Baker, R.; Liska, P.; Charvet, R.; Comte, P.; Nazeeruddin, M. K.; Pechy, P.; Takata, M.; Miura, H.; Uchida, S.; Grätzel, M. *Adv. Mater.* **2006**, *18*, 1202–1205.
(24) Hore, S.; Vetter, C.; Kern, R.; Smit, H.; Hinsch, A. *Sol. Energy Mater. Sol. Cells* **2006**, *90*, 1176–1188.
(25) Park, N. G.; van de Lagemaat, J.; Frank, A. J. *J. Phys. Chem. B* **2000**, *104*, 8989–8994.

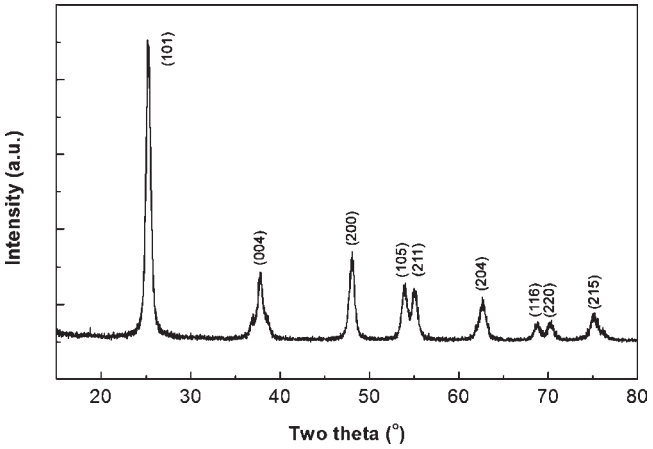

Figure 1. XRD pattern of the formed TiO_2 mesoporous spheres.

(http://www.wavemetrics.com/). The measurements were carried out at room temperature after allowing the cells to cool down and equilibrate for 30 min. The incident monochromatic photon to current conversion efficiency (IPCE) spectra were measured as a function of wavelength from 300 to 800 nm using an Oriel 300W xenon arc lamp and a lock-in amplifier M 70104 (Oriel) under monochromator illumination, which was calibrated with a monocrystalline silicon diode.

Results and Discussion

The phase purity of the products is characterized by XRD (Figure 1). The diffraction peaks identify the sample as anatase TiO_2 (JCPDS Card No. 21−1272). The peaks at scattering angles of 25.18, 37.78, 48.00, 53.89, 54.99, 62.57, 68.68, 70.15 and 75.01° correspond to the reflections from the 101, 004, 200, 105, 211, 204, 116, 220, and 215 crystal planes, respectively, of anatase TiO_2. The broadening of the diffraction peaks reveals the smaller particle size of the TiO_2 specimens. The average crystallite size roughly estimated based on the Scherrer formula is about 12 nm, implying that the mesospheres are composed of smaller nanocrystals.

The morphology and microstructure of mesoporous TiO_2 nanospheres are clearly demonstrated by TEM and HRTEM images. Typical TEM image for the mesoporous TiO_2 nanospheres shown in Figure 2a reveals that the sample consists of well-defined spherical structures, and the average size is about 216 nm. The well-defined spherical nature of the sample can be confirmed by the corresponding electron diffraction (ED) pattern (inset of Figure 2a), which shows diffuse rings, indicating that TiO_2 spheres are polycrystalline. The concentric rings could be assigned as diffraction from {101}, {004}, {200}, {211}, and {204} planes of anatase TiO_2 from the centermost ring, respectively. Figure 2b also gives randomly selected TEM image of a TiO_2 nanosphere, showing the well-defined spherical structure. The enlarged image is shown in Figure 2c. From this figure we observe that the nanosphere is constructed of nanoparticles about 12 nm in diameter, which is consistent with the XRD results. It should be noted that the sample exhibits mesoporous structure, and the wormlike nanopores with pore size of about 8 nm can be seen clearly forming the special closely interconnected nanostructures. Detailed analysis on the lattice fringes gives an interplanar spacing of 0.34 nm (inset of Figure 2c), which matches well with the (101) plane separation of the standard bulk anatase TiO_2.

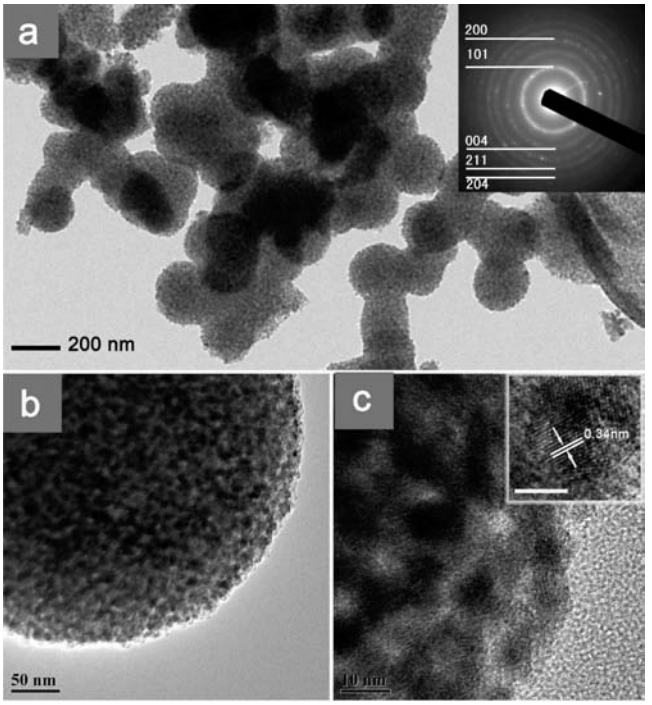

Figure 2. (a) TEM image of the formed mesoporous TiO_2 nanospheres. (b, c) Selected high-magnification TEM images of one TiO_2 mesoporous nanosphere. Inset of (a) shows the ED pattern of the sample.

From the high-resolution transmission electron microscopy (HRTEM) image (Figure 3), the parallel lattice fringes among almost all the primary building blocks and the grain boundaries can be seen clearly, which confirm the oriented aggregation of TiO_2 nanocrystals. The attached planes are not (001) with high surface energy but {101} with low energy. Previous papers have demonstrated that the order of the average surface energies of anatase TiO_2 is 0.90 J/m^2 for {001} > 0.53 J/m^2 for {100} > 0.44 J/m^2 for {101},[26,27] showing that the {101} crystal faces of anatase have a lower surface energy and are expected to be more stable than the others. Generally, oriented attachment may occur occasionally on (001), and rarely on {101} in common TiO_2 systems except in some special conditions, for example, the hydrothermal condition, crystal growth occurred along [001].[28] This mechanism effectively serves to reduce the overall surface energy by eliminating the surfaces at which the crystallites join. Lazzeri et al. have demonstrated that the surface density of 6-fold-coordinated Ti atoms with the hydroxyl of the (001) surface structure is high as compared to the {101} surface. The numbers of hydroxyl groups are 7.0 nm^{-2} for (001) surfaces and 5.1 nm^{-2} for {101} surfaces, respectively.[26] In this case, the (001) plane can be expected to adsorb many more groups (e.g., boron specimen) than the {101} plane and hindered the contact between (001) planes, resulting in oriented attachment occurring on the {101} plane. In DSSCs, using the oriented attachment structure as an eletrode film can decrease intercrystalline contacts among TiO_2 nanocrystals in comparison with a TiO_2 thin film composed of accumulated particles, which decrease the number of grain boundaries and electron traps in the photoelectrode. It could be a

(26) Lazzeri, M.; Vittadini, A.; Selloni, A. *Phys. Rev. B* **2002**, *65*, 119901.
(27) Diebold, U. *Surf. Sci. Rep.* **2003**, *48*, 53–229.
(28) Banfield, J. F.; Welch, S. A.; Zhang, H. Z.; Ebert, T. T.; Penn, R. L. *Science* **2000**, *289*, 751–754.

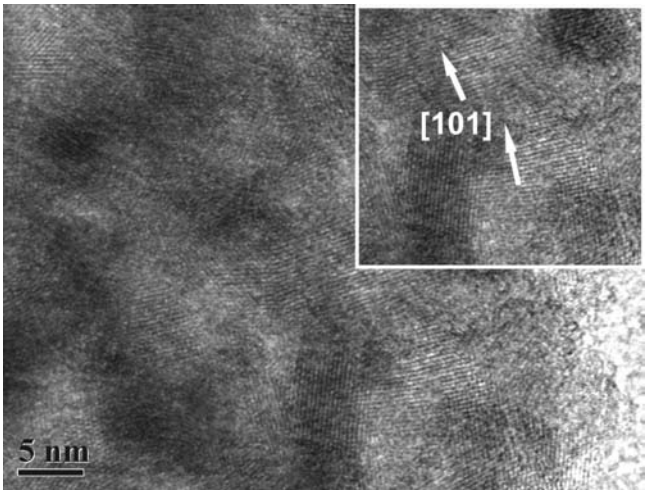

Figure 3. HRTEM image of the aggregated TiO_2 nanocrystals. The inset shows HRTEM image masked the {101} plane by the inverse FFT method.

Table 1. Summary of Experimental Conditions and Results of the Resultant Mesoporous TiO_2 Nanospheres[a]

	sample			
	A	B	C	D
boric acid/M	0	0.43	0.85	1.70
morphology[b]	P	P(S)	S	S(P)
average diameter/nm	9.8	10.6(266.0)	216.7	222.2 (11.2)
surface area/$m^2 \cdot g^{-1}$	45.32	138.90	153.00	98.99
pore size/nm	6.70	9.50	8.30	11.70
total pore volume/$cm^3 \cdot g^{-1}$	0.76	0.33	0.31	0.29

[a] In the above-mentioned experiments, 100 mL of water was used. [b] The letters P and S represent the particulate and spherical morphology, respectively. The letter in the bracket indicates the yield of the corresponding products is low in comparison with the counterpart outside the bracket.

benefit for easier electron transfer through the TiO_2 layer and suppression of back reaction of excited injected electrons.[29,30]

The morphology of the samples is found to be strongly dependent on the experimental conditions such as the interfacial reaction and concentration of boric acid. The parameter and influence on the morphology and structure of the samples are listed in Table 1. In the present system, there exists an interface of water/*n*-butanol, and TBT is apt to hydrolyze at the interface region between water and *n*-butanol. To understand the role of the interface of water/*n*-butanol on the formation of the spherical morphologies, we performed a series of controlled experiments. Without *n*-butanol, because of the absence of the interface, the TBT could hydrolyze rather homogeneously in the solution, and only mesoporous TiO_2 with irregular morphologies, not spheres, could be obtained. With *n*-butanol, TBT hydrolyzed at the interface region between water and *n*-butanol along with the formation of microsized droplets, which can be observed clearly when carrying out the experiments. These particles are further accumulated to form spherical TiO_2 mesostructures. These results confirm the crucial role of the

Scheme 1. Schematic Illustration of the Formation of Mesoporous Spherical TiO_2

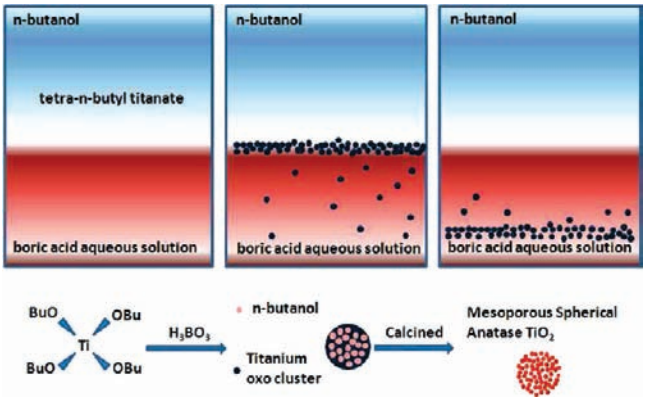

water/*n*-butanol interface on the formation of spherical TiO_2 mesostructures. The formation status of spherical TiO_2 mesostructures has also been found to be strongly dependent on the utilization of boric acid. Without boric acid, the morphology of the samples varied greatly, and then only TiO_2 nanoparticles can be obtained (Supporting Information, Figure S1). By fine-tuning of boric acid concentration, the evolution from monodispersed nanocrystals to aggregated mesoporous nanospheres can occur. When the boric acid concentration was 0.43 M and the other experimental conditions were the same as in the typical synthesis, the TiO_2 nanocrystals exhibited the aggregation tendency and some irregular TiO_2 nanospheres formed (Supporting Information, Figure S2). With increase in boric acid content up to 0.85 M, well-defined mesoporous TiO_2 nanospheres formed (Figure 2). When the boric acid content supersaturated (even up to 1.7 M), the sample still exhibited spherical morphology along with the formation of some individual TiO_2 nanocrystals (Supporting Information, Figure S3).

Synthesis of nanostructured materials based on interfacial confined formation is intriguing as interfaces are able to break symmetry and enrich the components from bulk solutions as well as provide nucleation sites.[31−35] Zhang et al. utilized hard interfaces between metal foils and aqueous solutions to grow oriented nanostructured films of metal chalcogenides.[32] We would like to propose a possible formation process as shown in Scheme 1. The TBT hydrolyzed into an amorphous TiO_2 sol at the beginning of the reaction quickly at the interface region, which gradually ripens into the well-defined TiO_2 nanoparticles with aging. As diffusion-limited aggregation mostly leads to disordered particles with no structural porosity, the present reaction is believed to proceed via reaction-limited aggregation, where only a small fraction of the collisions result in the two particles involved adhering to each other.[36,37] The boric acid solution maybe

(29) Adachi, M.; Murata, Y.; Takao, J.; Jiu, J. T.; Sakamoto, M.; Wang, F. M. *J. Am. Chem. Soc.* **2004**, *126*, 14943–14949.
(30) Chi, Q. J.; Zhang, J. D.; Andersen, J. E. T.; Ulstrup, J. *J. Phys. Chem. B* **2001**, *105*, 4669–4679.
(31) Xu, H.; Jia, F. L.; Ai, Z. H.; Zhang, L. Z. *Cryst. Growth Des.* **2007**, *7*, 1216–1219.
(32) Zhang, L. Z.; Yu, J. C.; Mo, M. S.; Wu, L.; Li, Q.; Kwong, K. W. *J. Am. Chem. Soc.* **2004**, *126*, 8116–8117.
(33) Song, X. Y.; Sun, S. X.; Zhang, W. M.; Yu, H. Y.; Fan, W. L. *J. Phys. Chem. B* **2004**, *108*, 5200–5205.
(34) Lin, Y.; Skaff, H.; Emrick, T.; Dinsmore, A. D.; Russell, T. P. *Science* **2003**, *299*, 226–229.
(35) Wang, D. Y.; Duan, H. W.; Mohwald, H. *Soft Matter* **2005**, *1*, 412–416.
(36) Zhou, Y.; Antonietti, M. *J. Am. Chem. Soc.* **2003**, *125*, 14960–14961.
(37) Family, F.; Landau, D. *Kinetics of Aggregation and Gelation*; North-Holland: Amsterdam, 1984.

favors the reaction-limited aggregation of the formed TiO_2 nanoparticles via specific sides. As known from hydrothermal synthesis of TiO_2 nanoparticles,[38] these specific faces of the nanoparticles can then fuse to minimize the interface energy. The well-defined structural porosity of the present spherical TiO_2 aggregate would then result from the tensorial reaction-limited aggregation probability, branching the rates and the defects involved.[36] By adjusting the concentration of boric acid used, the pH value of the solution varied, which could influence the hydrolysis rate as well as the motion of the formed TiO_2 nanoparticles. Without boric acid, although there exists a water/*n*-butanol interface, vigorous hydrolysis reaction of TBT could take place inevitably along with the dropping of TBT to the solution. However, after introducing boric acid, the hydrolysis of TBT was restricted, and the interface supplied an ideal hydrolysis region. After ripening into the TiO_2 nanoparticles, the aggregation took place. Spherical emulsions formed in this interface region may serve as aggregation centers for the primary colloid particles.[39] Through the reaction-limited aggregation and spherical emulsion template, mesoporous spherical aggregates could be formed. At an optimal boric acid concentration (e.g., ~0.85 M), the products are all mesoporous spherical aggregates. If the concentration was further increased (e.g., ~1.70 M), both hydrolysis speed and motion of TiO_2 nanoparticles slowed down. As found in our experiments, products composed of irregular mesostructures and nanoparticles were formed.

Brunauer−Emmett−Teller (BET) measurement were performed to understand the three-dimensional (3D) distribution of the mesoporous TiO_2 spheres and determine the specific surface area.[16] From the specific surface areas shown in Table 1 a similar tendency can be found in comparison with TEM results; the specific surface area of the product increased drastically from 45.32 to 153.00 m^2/g when the morphology of the product varied from individual nanocrystals to mesoporous spheres. In the case of a saturated solution of boric acid, the specific surface area of the product decreased greatly to 98.99 m^2/g because not all TiO_2 nanoparticles were aggregated to form mesoporous TiO_2 spheres.

To obtain the insight information about the textural properties of the synthesized mesoporous TiO_2, the N_2 adsorption−desorption measurement at a liquid N_2 temperature of −196 °C was carried out (Figure 4). Nitrogen adsorption−desorption isotherms of the samples exhibited typical IUPAC type IV sorption behavior with hysteresis loops, ascribed to the existence of the mesoporous structure. A sharp increase in the adsorption volume of N_2, located in a relative pressure range about 0.5−0.9, was observed when boric acid was introduced. This sharp increase can be assigned to the capillary condensation, indicating good homogeneity of the samples and fairly small pore sizes. Pore size distributions for the discussed samples, calculated from the nitrogen desorption isotherms using the BJH method, are illustrated in the inset of Figure 4. To better show the full range of relevant pore diameters, the logarithmic scale was used. The patterns implied the mesoporous TiO_2 with narrow pore size distribution.

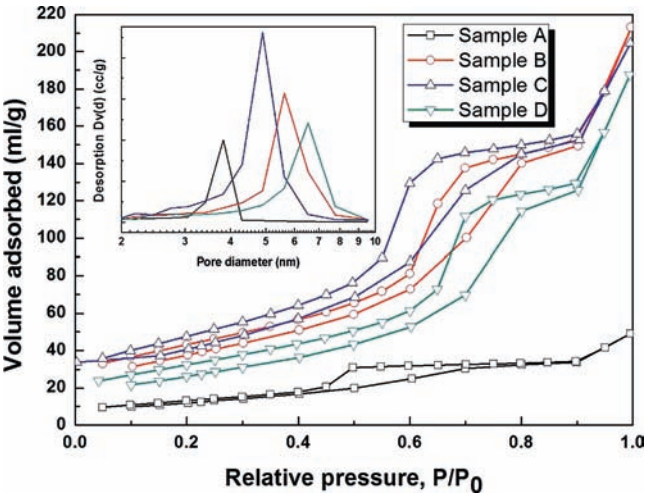

Figure 4. Nitrogen absorption−desorption isotherms and pore size distribution plots (inset) of the mesoporous TiO_2 materials.

To establish the relationship between structural characteristics of the sample and the cell performance, we tentatively investigated the porosity (P) and surface roughness factor (R) based on the BET measurements of the calcined samples. The porosities can be calculated by using the following equation:[16,40] $P = V_p/(q^{-1} + V_p)$, where V_p is the specific cumulative pore volume ($cm^3 \cdot g^{-1}$) and q is the density ($g \cdot cm^3$) of anatase TiO_2, which were approximately 74.7%, 56.2%, 54.7%, and 53.0%, respectively, showing that the products have a large porosity and the pores constitute more than half of the volume. The porosity in nanocrystalline TiO_2 films employed in DSSCs is typically in the range of 50−65%.[40] The porosities of the prepared mesoporous products were exactly in this range. An estimation of R could be induced by the following equation:[41] $R = q(1 - P)S$, where P is the porosity (%), and S is the specific surface area (m^2/g). The calculated roughness factors (μm^{-1}) were approximately 42.3, 362.1, 410.8, and 273.5 for these four samples, respectively, showing that the mesoporous samples have much higher dye adsorption ability, which would lead to an obvious increase in the charge harvesting efficiency from a larger amount of dye adsorption.

FT-IR and X-ray photoelectron spectroscopy (XPS) are used to detect whether or not the B element exists in TiO_2 mesoporous samples. FT-IR spectra (Figure 5a) of the formed mesoporous TiO_2 nanospheres shows very weak absorption at 1381 cm^{-1} ascribed to tri-coordinated boron.[42] B1s and Ti2p XPS spectra of the sample are shown in Figure 5b. Because of the XPS measurement sensitivity and low boron amount, the B1s peak at about 191.4 eV is weak and, to some extent, can be influenced by instrument noise.[43,44] This suggests that there is little boron vestige in the formed TiO_2 mesoporous sphere, which has no marked influence on the performance of the material.

(38) Penn, R. L.; Banfield, J. F. *Geochim. Cosmochim. Acta* **1999**, *63*, 1549–1557.
(39) Fei, H. L.; Liu, Y. P.; Li, Y. P.; Sun, P. C.; Yuan, Z. Y.; Li, B. H.; Ding, D. T.; Chen, T. H. *Microporous Mesoporous Mater.* **2007**, *102*, 318–324.
(40) van de Lagemaat, J.; Benkstein, K. D.; Frank, A. J. *J. Phys. Chem. B* **2001**, *105*, 12433–12436.
(41) Benkstein, K. D.; Kopidakis, N.; van de Lagemaat, J.; Frank, A. J. *J. Phys. Chem. B* **2003**, *107*, 7759–7767.
(42) On, D. T.; Kaliaguine, S.; Bonneviot, L. *J. Catal.* **1995**, *157*, 235–243.
(43) Li, J. Y.; Lu, N.; Quan, X.; Chen, S.; Zhao, H. M. *Ind. Eng. Chem. Res.* **2008**, *47*, 3804–3808.
(44) Zhao, W.; Ma, W. H.; Chen, C. C.; Zhao, J. C.; Shuai, Z. G. *J. Am. Chem. Soc.* **2004**, *126*, 4782–4783.

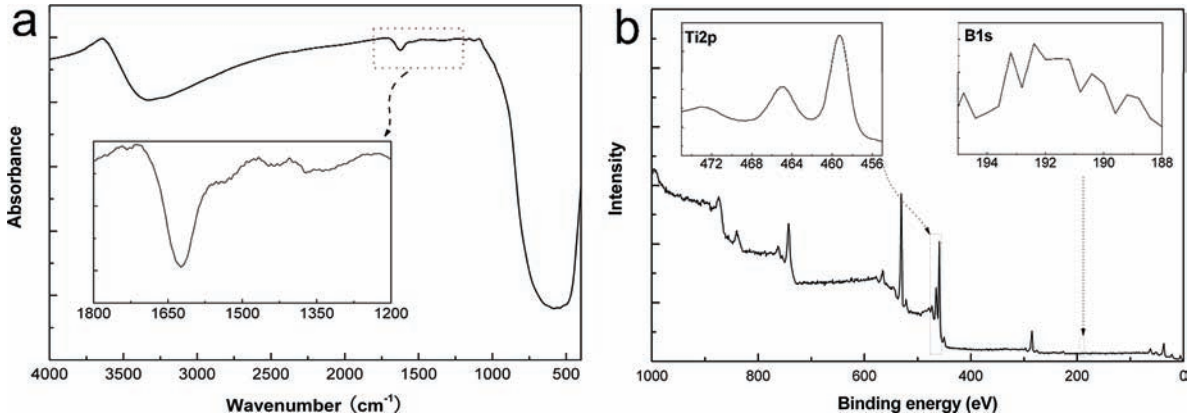

Figure 5. (a) FT-IR spectra of the formed TiO_2 mesoporous spheres and (b) XPS spectra of the obtained mesoporous spherical TiO_2 samples.

Table 2. Summary of the Photovoltaic Characteristics of the TiO_2 Bilayer Films[a]

cell	J_{SC} mA·cm^{-2}	V_{oc} V	FF	η %	adsorbed dye $\times 10^{-7}$ mol cm^{-2}[,b]
A	11.77	0.80	0.58	5.43	1.45
B	14.97	0.73	0.59	6.47	1.91
C	17.00	0.75	0.61	7.79	2.39
D	13.69	0.73	0.63	6.34	1.64
E	11.70	0.80	0.64	6.00	1.25

[a] Cells A−D were fabricated by using the Samples A−D listed in Table 1, respectively, composed of P25-TiO_2 underlayer and mesoporous spherical TiO_2 overlayer. Cell E was composed of double P25-TiO_2 layers. Measurements were performed under AM 1.5G one sun light intensity of 100 mW·cm^{-2} and the active areas were about 0.25 cm^2 for all of the cells. [b] Dye-adsorbed films with a dimension of 0.25 cm^2 were used for estimating the adsorbed dye concentration.

To investigate the effect of the structural characteristics of TiO_2 on the cell performance, DSSCs based on mesoporous spherical and nanoparticulate TiO_2 films were fabricated. The mesoporous spherical TiO_2 layer was formed on a P25-derived semitransparent TiO_2 film (~4 μm). Table 2 summarizes the photovoltaic characteristics of the TiO_2 films composed of a P25-TiO_2 layer and as-prepared TiO_2 overlayer. For comparison, the characteristic of double P25-TiO_2-layer-based film is also included. The cross-sectional SEM image of this kind of bilayer structure is shown in Figure 6 with the thickness of about 15 μm. The mesoporous TiO_2 layer is loose, resulting in high dye adsorption and light scattering. The P25-TiO_2 layer is compact and be a benefit for contact with the substrate. From Table 2 and Figure 7, it can be found that the conversion efficiency as well as the short-circuit photocurrent density increased remarkably along with the formation of mesoporous spherical samples. In the case of particulate TiO_2 (Cell A), the conversion efficiency (η) and short-circuit photocurrent density (J_{SC}) are 5.43% and 11.77 mA·cm^{-2}, respectively. With the formation of mesoporous spherical TiO_2 in the sample, both η and J_{SC} are increased. The higher J_{SC} is probably related to either the amount of adsorbed dye or the light scattering or both. When the samples are totally composed of mesoporous spherical TiO_2 (Sample C), the conversion efficiency reaches 7.79%, corresponding to over 43% increment in comparison with Sample A. In comparison with Cell E (double P25-TiO_2), Cell C exhibits a higher short-circuit photocurrent density (J_{SC}). For Sample D, the formation of particulate TiO_2 weakens the function of the mesoporous products; therefore, both η and J_{SC} are decreased. The amount of adsorbed dye for the

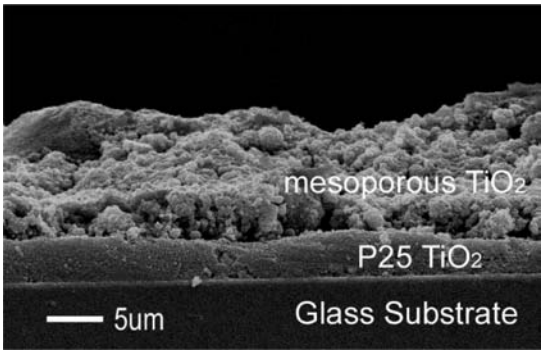

Figure 6. Cross-sectional SEM image of a bilayer structure showing P25-TiO_2 underlayer and the mesoporous spherical TiO_2 overlayer.

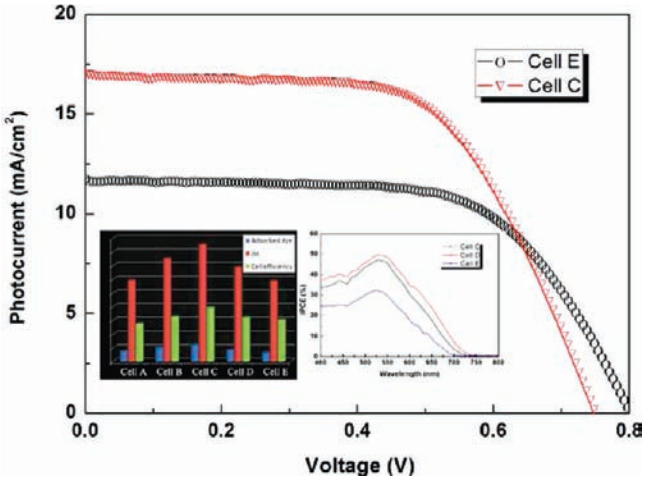

Figure 7. $J-V$ characteristics of TiO_2-based dye-sensitized solar cells. The insets show evolution tendency of the values of dye adsorbed, J_{SC} and η of the obtained cells and IPCE spectra of the cells.

films can give a similar tendency. With the formation of mesoporous spherical TiO_2 (increasing surface area), the amount of dye adsorbed rises drastically from 1.45×10^{-7} mol·cm^{-2} to 2.39×10^{-7} mol·cm^{-2}. Therefore, the higher J_{SC} observed for mesoporous spherical TiO_2 is attributed to the larger quantity of dye on the mesoporous spherical particles, which is consistent with the calculated roughness factors results from BET measurements. The good performance of the DSSCs fabricated with mesoporous spherical TiO_2 may come from the crystal morphology and surface

orientation of anatase TiO_2. Upon the formation of the mesoporous structure, the specific surface area of the sample increases gradually. The higher J_{SC} is expected because of the increased amount of adsorbed dye. The special spherical morphology processing light-scattering characteristics will also benefit the cell performance. As illustrated in the incident photon-to-electron conversion efficiency (IPCE) spectra in the inset in Figure 7, it is observed that both Cell C and Cell D had a higher IPCE from 400 to 750 nm compared with Cell E, implying improved light utilization efficiency from these special light-scattering structures of the mesoporous TiO_2 spheres. Besides these, the mesoporous structure based on the oriented attachment of TiO_2 nanocrystals plays a critical role in optimizing the cell performance. The intercrystalline TiO_2 contacts are greatly decreased by forming such network structure in comparison with a porous TiO_2 thin film composed of accumulated nanosize particles, which might be a benefit for electron transfer through the TiO_2 layer, suppression of back reaction of photoinjected electrons with I_3^-, and also high dye adsorption on the TiO_2 surface. Thereby, better cell performance based on this mesoporous spherical structure is exhibited.

Conclusions

In summary, we have prepared mesoporous spherical TiO_2 and investigated their photovoltaic properties in dye-sensitized solar cell. The mesoporous spherical structure was found to be composed of oriented-attached TiO_2 nanocrystals. Because of the special spherical and mesoporous structures, better cell performance can be obtained by enhancing the amount of adsorbed dye and light scattering when using as a secondary layer in dye-sensitized solar cells. Such mesoporous spherical TiO_2 can be utilized as an efficient material for high-efficiency dye-sensitized solar cells.

Acknowledgment. This work was supported by the National Natural Science Foundation of China (20925621, 20906027, 20706015), the Program of Shanghai Subject Chief Scientist (08XD1401500), the Shanghai Rising-Star Program (09QH1400700, 09QA1401500), the Special Projects for Key Laboratories in Shanghai (09DZ2202000), the Special Projects for Nanotechnology of Shanghai (0852 nm02000, 0952 nm02100), and the Alexander von Humboldt Foundation.

Supporting Information Available: TEM image of TiO_2 sample prepared without boric acid (Figure S1). TEM image of the TiO_2 sample prepared with 0.43 M boric acid concentration (Figure S2). TEM image of the TiO_2 sample prepared with 1.70 M boric acid (Figure S3). This material is available free of charge via the Internet at http://pubs.acs.org.